Boundary-Layer Meteorology (2006) 119: 135–157
DOI 10.1007/s10546-005-9005-9


# MIXED-LAYER DEPTH DETERMINATION IN THE BARCELONA COASTAL AREA FROM REGULAR LIDAR MEASUREMENTS: METHODS, RESULTS AND LIMITATIONS

M. SICARD[1,*], C. PÉREZ[2], F. ROCADENBOSCH[1], J.M. BALDASANO[2] and D. GARCÍA-VIZCAINO[1]

[1] *Universitat Politècnica de Catalunya, Dept. de TSC, Jordi Girona 1, 08034 Barcelona, Spain*
[2] *Universitat Politècnica de Catalunya, LMA, Avda. Diagonal 647, planta 10, 08028 Barcelona, Spain*

(Received in final form 11 July 2005 / Published online: 17 December 2005)

**Abstract.** Regular aerosol backscatter measurements using an elastic-backscatter lidar were performed between May 2000 and December 2002 in Barcelona (Spain), within the framework of the European project EARLINET (European Aerosol Research Lidar Network). The mixed-layer depth was one of the major parameters to be retrieved. Three derivative methods have been tested in this complex coastal area using the range-squared-corrected lidar signal: (1) the minimum of its first derivative, (2) the minimum of its second derivative, and (3) the minimum of the first derivative of its logarithm. The second method was found to give statistically the best results when compared to radiosoundings, and was used to process the whole dataset. A number of 162 days and 660 profiles averaged over 30 min have been examined. Between 1000 and 1500 UTC, the mixed-layer depth oscillates between 300 and 1450 m in summer and between 390 and 1420 m in winter. The standard deviation for this portion of the day is 180 and 256 m, respectively, in summer and winter. In summer, low heights (mainly limited to 400–800 m) are associated with large mesoscale compensatory subsidence over the sea and to the thermal internal boundary-layer formation. The strong coastal and orographic influences and the climatological settling of Barcelona determine the complexity of the boundary-layer dynamics and the high heterogeneity of the lidar signals. In many cases, single lidar analyses do not allow an unambiguous determination of the mixed-layer depth. Two diurnal cycle measurements are discussed together with synoptic maps, backtrajectories and radiosoundings in order to outline the complexity of the area and the limitations of the methods.

**Keywords:** Coastal region, Complex terrain, Lidar profiles, Mixed-layer depth, Radiosoundings.

## 1. Introduction

The atmospheric boundary layer (ABL) has a thickness quite variable in space and time, ranging from a hundred of metre or so to a few kilometres.

* E-mail: msicard@tsc.upc.edu

In convective conditions in particular, pollutants that are emitted into the mixed layer (ML) become gradually dispersed and mixed through the action of turbulence; the mixed-layer depth (MLD) is a key parameter, and is also called the mixing height (Seibert et al., 1998, 2000). Measurements, parameterizations and predictions of the MLD have many theoretical and practical applications such as the prediction of pollutant concentrations and surface temperature, the scaling of turbulence measurements or the treatment of the ML in numerical weather prediction and climate models (Seibert et al., 1998). Different ways exist to determine or estimate the MLD. During daytime, radiosoundings are the most common data source to retrieve the MLD based on wind, temperature and pressure profiles but at most stations regular launches are made only twice a day at pre-determined synoptic times (0000 and 1200 UTC).

Active remote sensing systems such as lidars use aerosols as tracers, with the optical power measured by a lidar proportional to the aerosol content of the atmosphere. The lidar signal shows strong backscattering within the ML, which decreases through a transition zone and becomes weak in the free troposphere (FT). These contrasts are the basis for the lidar estimates of the MLD. Under convective conditions, the ABL can be divided into three different layers: the surface layer, the ML and the entrainment zone (EZ). The last represents a transition zone between the ML and the stable atmosphere (FT) above, and usually the EZ is defined in a horizontal average sense (Deardorff et al., 1980). It is important to distinguish between the instantaneous (or local) MLD that varies between the EZ top and the middle of the ML and the average MLD defined as the middle of the EZ (Stull, 1988). Ground-based aerosol lidars give a high-resolution picture of the instantaneous ML top that is marked by a large contrast between the backscatter signal from aerosol-rich structures below and cleaner air above. This lidar transition zone should not be confused with the classical definition of the EZ defined by Deardorff et al. (1980) given above. Furthermore, it is worth noting that the lidar-derived transition zone, usually assumed to correspond closely with the temperature inversion, does not respond directly to the thermodynamic properties of the atmosphere: it can only be assumed to be a proxy for the temperature inversion (Brooks, 2003).

However, interpreting observations from lidars is often not straightforward, because the detected layers are not always the result of ongoing vertical mixing, but may originate from advective transport or past accumulation processes (Seibert et al., 2000). In our case, Barcelona is a coastal city located in the north-eastern Iberian peninsula (IP) and surrounded by complex orography. The meteorology and the origin of the air masses arriving at the IP are highly influenced by the Azores anticyclone that is usually located over the Atlantic Ocean. The more usual synoptic situations affecting the

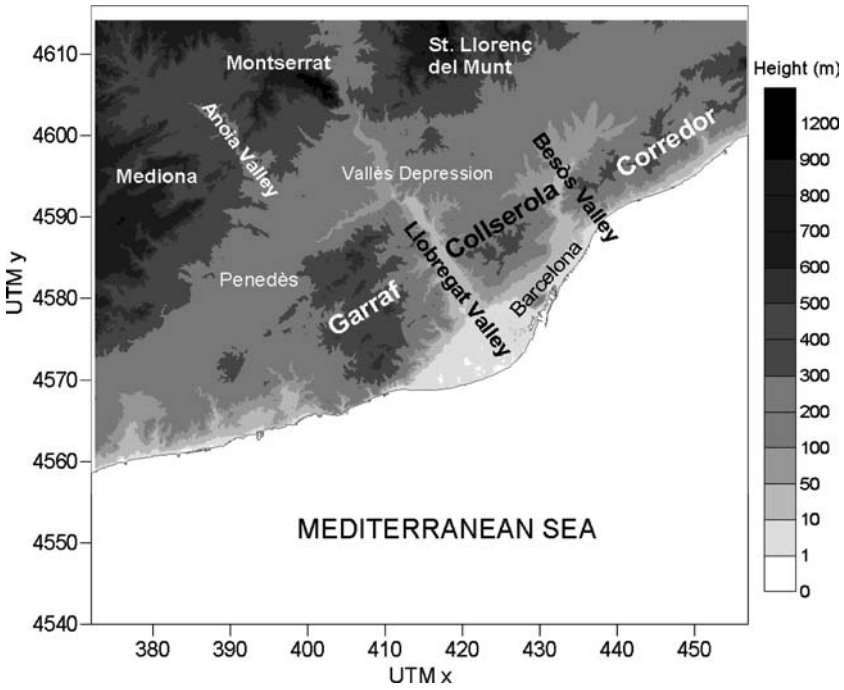


*Figure 1.* Orography of the Barcelona geographical area. Coastal Mountains: Garraf, Collserola and Corredor. Pre-coastal mountains: Mediona, Montserrat and St. Llorenç del Munt.

Barcelona area are westerly and north-westerly flows in winter, and typical summertime weak pressure gradients (Martín-Vide, 1987; Jorba et al., 2004; Pérez et al., 2004). Under the latter conditions, mesoscale phenomena modify the ML flow generating circulations in conjunction with diurnal heating cycles. A thermal internal boundary layer (TIBL) forms and increases in depth to merge eventually with the ML at some distance from the coastline (Soriano et al., 2001). The nearby orography of the region shown in Figure 1 is dominated by four main features arranged parallel to the coastline: the coastal plain, the coastal mountain range (500–700 m), the pre-coastal depression, and the pre-coastal mountain range (700–1700 m). In summer, under strong insolation and weak synoptic forcing, sea breezes and mountain-induced winds develop to create re-circulations of pollutants along the eastern Iberian coast. Layers are formed when aerosols are injected from the mountains into the return flow at various heights and distances from the coast (Millán et al., 1997; Soriano et al., 2001; Barros et al., 2003; Pérez et al., 2004). In addition, the synoptic scale meteorology induces frequent outbreaks of Saharan dust in summer (Rodríguez et al., 2001; Pérez et al., 2003).

Several approaches have been used to estimate the MLD from lidar. Melfi et al. (1985) and Boers et al. (1988) used simple signal threshold values, though this method suffers from the need to define them appropriately taking into account variations in the signal strength within the dataset. Hooper and Eloranta (1986) used the height of the maximum of the variance of the lidar signal, whilst some authors noted that the results tended to be biased to higher altitudes due to humidity effects (Dupont et al., 1991; Menut et al., 1999). Derivative methods are the most common – a total of three are known: Hayden et al. (1997) and Flamant et al. (1997) used the largest negative peak of the first derivative of the lidar signal as a marker for the instantaneous MLD. Menut et al. (1999) compared the absolute minimum of the second derivative of the lidar signal with the maximum of the standard deviation profile of the signal and found that the latter method overestimated the MLD when compared to radiosoundings. In a similar way, Senff et al. (1996) used profiles of the derivative of the logarithm of the lidar signal. Steyn et al. (1999) fitted an idealized profile to define the ML top and the transition zone depth, but Hägeli et al. (2000) found that the technique produced biased results for complex backscatter profiles. Cohn and Angevine (2000) used a wavelet-based technique providing a scale-dependent gradient locator. The results were biased by gradients in the background signal. Recently, Brooks (2003) developed an alternative approach using multiple wavelet dilatations and capable of identifying the upper and lower limits of the transition zone remaining insensitive to vertical gradients.

Within the framework of the European project EARLINET (European Aerosol Research Lidar Network) (Bösenberg et al., 2001, 2003), Barcelona and 20 European lidar stations performed regular lidar measurements from May 2000 to December 2002 to provide a climatological database of the vertical and horizontal distribution of aerosols over Europe. Among other subjects, the network studied the aerosol properties in the lower troposphere and more particularly in the ABL at different time scales (diurnal and seasonal cycles). In this context, the MLD was one of the major parameters to be retrieved. Under the rather different conditions of the EARLINET stations, most reasonable suggestions pointed out the use of the three derivative methods, which can be applied to single lidar profiles as well as to averaged lidar profiles. This fact is important when the signal-to-noise ratio is not high enough or if one wants to reduce data flow (in both cases, temporal averaging is required) (Menut et al., 1999).

The objective of our study is to decide on the best of these three methods and to establish the criteria necessary for its application in order to extract a MLD climatology. The paper is organized as follows: the lidar system, the pre-processing of the measurements from EARLINET and the methods are presented in Section 2. In Section 3.1 the lidar-derived MLDs

are compared to objective radiosounding retrievals in order to find the best proxy value. Section 3.2 discusses some typical cases together with complementary data pointing out the application criteria and the limitations of the methods. In Section 3.3, the results from the whole database are presented and discussed.

## 2. Data and Methods

### 2.1. Lidar data and Earlinet

A transportable, steerable lidar system allowing three-dimensional scans has been developed at the Universitat Politècnica de Catalunya (UPC) (Rocadenbosch et al., 2002). The present system is based on a Nd:YAG laser working at the 1064-nm fundamental wavelength and at the 532-nm second harmonic, delivering pulses of equal energy (160 mJ) and 6-ns duration with a 20 Hz pulse repetition frequency (PRF). The photoreceiver is based on an avalanche photodiode (APD) with a wide spectral response (its quantum efficiency is about the same at both wavelengths). The wavelength is changed by placing manually the corresponding interference filter in front of the APD. The emission and reception axes are different so that a blind zone is observed between 0 and 250 m. However, the overlap factor reaches 1 rapidly.

In the framework of EARLINET, regular lidar measurements were undertaken from May 2000 to December 2002 on preselected dates regardless of weather conditions (Bösenberg et al., 2001, 2003). To this end, a common schedule of three measurements per week was agreed. Measurements were performed on Mondays at 1400 LST (local standard time) $\pm 1$ h and at sunset (2 h before to 2 h after) on Mondays and Thursdays. Furthermore, the network performed diurnal cycle measurements under unperturbed weather conditions, ideally under high-pressure conditions, to allow simultaneous observations at different stations and quantify the behaviour of aerosols at the regional scale.

All lidar measurements were made at the UPC campus, south–west of Barcelona (41.39° N, 2.12° E, 115 m above sea level), at a wavelength of 532 or 1064 nm; sequences of 1-min duration (1200 shots) were recorded. In this analysis, $X$-minute integrated profiles refer to the average of $X$ consecutive 1-min profiles. In Section 2, for the methods' validation, $X = 15$ min is taken for optimizing the matching time between lidar and radiosoundings measurements, and reducing the difference that could arise by integrating lidar profiles for too long. In Section 3, in order to comply with the EARLINET rules and reduce the quantity of data, the EARLINET database was processed with $X = 30$ min.

### 2.2. Methods used in the determination of the MLD from lidar data

The optical power measured by a lidar is proportional to the signal backscatter from particles and molecules present in the atmosphere. The lidar signal can be expressed as:

$$S(r) = \frac{K}{r^2}\left[\beta^{\mathrm{a}}(r) + \beta^{\mathrm{m}}(r)\right] T(r)^2 + S_0 \tag{1}$$

where $\beta^a$ and $\beta^m$ are, respectively, particular and molecular backscatter coefficients, $K$ is the system constant, $T$ is the atmospheric transmission, $r$ is the distance between the laser source and the target (it is also called range), and $S_0$ is the background signal. The range-squared-corrected signal (RSCS) is then defined as:

$$\mathrm{RSCS} = (S - S_0) r^2. \tag{2}$$

For the marked transition between the ML and the FT, the derivative of RSCS exhibits a strong negative peak. The first of the three derivative methods used to estimate the MLD is the gradient method (GM); this searches for the altitude ($\mathrm{h}_{GM}$) of the absolute negative minimum of the first derivative of the RSCS,

$$h_{\mathrm{GM}} = \min\left[\frac{\partial \mathrm{RSCS}}{\partial r}\right]. \tag{3}$$

However, in complex profiles several minima exist over an extended height range and the absolute minimum does not always give the MLD but the height of the top of an upper layer. In the morning, it becomes necessary to distinguish between the newly developed ML and the residual layer (RL) from the day before. When both the ML and the RL exist together, these layers are typically well disconnected and two local negative minima (i.e. the first derivative crosses the $x = 0$ axis between them) can be observed. This two-layer effect is described by Stull (1988). In other frequent situations over Barcelona, one or more layers of advected aerosols can be found on top of the ML. In all cases, if several layers that are separated (i.e. the first derivative crosses the $x = 0$ axis) exist, only the lowest layer is identified as the ML. The difficulty is then to determine the lowest negative peak. Since RSCS is noisy, and the atmosphere is particularly variable when reaching the MLD, the derivative of the RSCS can present several small negative peaks; a criterion that eliminates non-significant peak is to define a transition zone for every peak and compare it to a minimum depth (Flamant et al., 1997). The depth of this zone is the height difference between the highest and the lowest data point. A peak is considered representative if its associated transition zone includes a minimum of five points.

The inflection point method (IPM) looks for the altitude, $h_{\mathrm{IPM}}$, where the inflection point of the first derivative occurs. While Menut et al. (1999) used the absolute minimum of the second derivative, in the present study $h_{\mathrm{IPM}}$ corresponds to the minimum of the second derivative of the RSCS located just below $h_{\mathrm{GM}}$,

$$h_{\mathrm{IPM}} = \min\left[\frac{\partial^2 \mathrm{RSCS}}{\partial r^2}\right]. \tag{4}$$

It is important to note that, so defined, $h_{\mathrm{IPM}}$ is not independent of $h_{\mathrm{GM}}$ unless the GM fails. In this case, $h_{\mathrm{IPM}}$ corresponds to the lowest negative peak of the second derivative. The criterion that $h_{\mathrm{IPM}}$ must be less than $h_{\mathrm{GM}}$ (when the GM detects correctly the "real" transition zone between the ML and the FT) arises from the fact that the second derivative of RSCS is a function changing sign each time the first derivative of RSCS changes direction. Consequently, the second derivative of RSCS tends to cross the $x = 0$ axis more times than the first derivative and therefore to exhibit various minima below and above $h_{\mathrm{GM}}$. The experience shows that the best estimator of the MLD is the minimum located just below $h_{\mathrm{GM}}$.

The derivative of the logarithm of RSCS is proportional to the aerosol extinction gradient and therefore it can also be used to detect the largest negative gradient. The logarithm gradient method (LGM), consists in finding the altitude, $h_{\mathrm{LGM}}$, at which the minimum of the first derivative of the logarithm of the RSCS is reached,

$$h_{\mathrm{LGM}} = \min\left[\frac{\partial \ln(\mathrm{RSCS})}{\partial r}\right]. \tag{5}$$

### 2.3. Radiosoundings

Each day the Meteorological Service of Catalonia performs two radiosoundings at 0000 and 1200 UTC from the Department of Astronomy and Meteorology of the University of Barcelona, at less than 500 m from the lidar station. Given its ascent rate (4–8 m s$^{-1}$), the balloon is considered to reach the ML top in less than 3 min. At 1200 UTC, the lidar 30-min integrated profiles show differences against 5- and 15-min integrated profiles. Since the exact time of the radiosounding launches is uncertain, an analysis of the 5-min integrated profiles could lead to large errors in the comparison with the radiosoundings due to not-matching measurement times. Therefore, 15-min integrated lidar profiles with starting times around 1200 UTC were chosen as a good compromise for comparison with available radiosoundings.

The bulk Richardson number method can be used in convective conditions to define the MLD. The Richardson number, $R_{\mathrm{ib}}$, is calculated as a

function of altitude $z$ as:

$$R_{\mathrm{ib}}(z) = \frac{g(z - z_0)}{\theta(z)} \frac{[\theta(z) - \theta(z_0)]}{[u(z)^2 + v(z)^2]}, \tag{6}$$

where $g$ is the acceleration due to gravity, $z_0$ the height of the surface above sea level, $\theta$ the potential temperature, and $u$ and $v$ the zonal and meridian wind components, respectively. The MLD is defined as the height where the Richardson number becomes equal to the so-called critical bulk Richardson number, $R_{\mathrm{ibc}}$, i.e. where $R_{\mathrm{ib}} = R_{\mathrm{ibc}}$. A value of 0.21 is taken for $R_{\mathrm{ibc}}$ (Vogelezang and Holtslag, 1996; Menut et al., 1999). Beyond this critical value of $R_{\mathrm{ib}}$ the atmosphere can be considered fully decoupled from the ML.

For the same time period (May 2000–December 2002), Sicard et al. (2003) compared the Richardson method with the simple parcel method (Holzworth, 1967) and found that the agreement was very good, even though the simple parcel method gave slightly lower heights due to its limitations in situations dominated by mechanical turbulence. Thus, lidar profiles were compared to the MLD retrieved by the Richardson number method.

## 3. Results and Discussion

### 3.1. Comparison of the MLD retrievals from lidar measurements and the Richardson number method

For the measurement period, 29 simultaneous radiosoundings and lidar measurements are available, but only 20 lidar profiles were processed by the three analysis methods. The reasons for discarding the other nine cases are the following:

- Cumulus clouds with little vertical extent and seemingly flattened have formed at the ML top,
- The MLD is underneath the useful lidar signal (before the overlap reaches 1),
- One of the methods exhibits too many negative peaks without crossing the $x = 0$ axis,
- An aerosol layer on top of the ML is coupled with the ML.

Cloud screening was applied to all of the 1-min integrated profiles by discarding the profiles featuring a positive gradient larger than a given threshold. In some cases, the MLD could not be determined simply because it was below or around 300 m, which is the altitude below which the overlap factor between the receiver field-of-view and the illuminated atmospheric

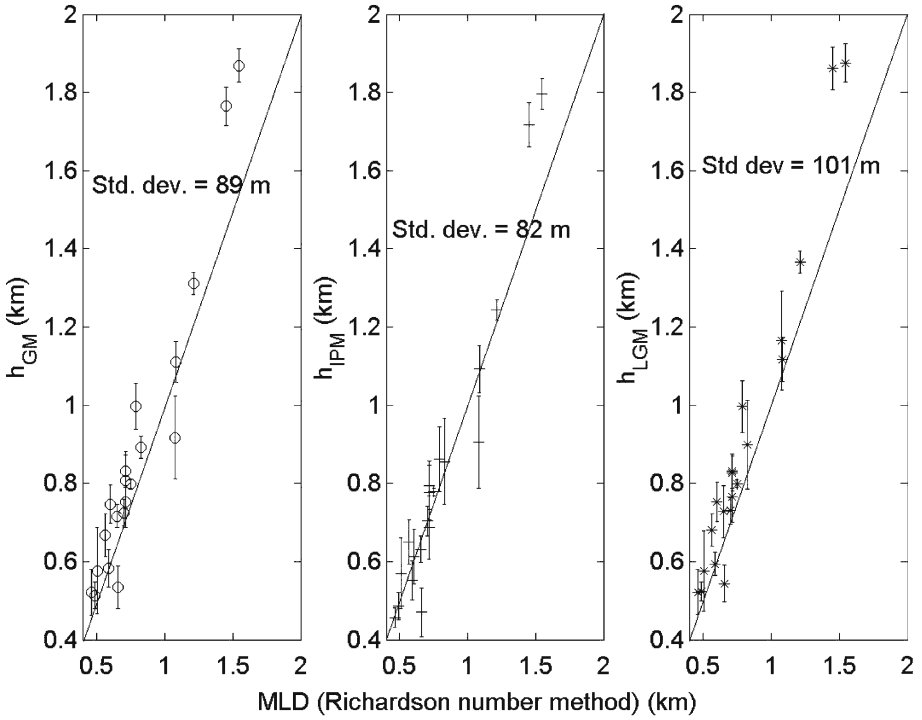


*Figure 2.* Comparison of $h_{GM}$, $h_{IPM}$ and $h_{LGM}$ with the MLD retrieved from radiosoundings using the Richardson number method. The standard deviation is reported in the middle of the figure for each method.

cross-section is still increasing to reach the stationary value, which distorts the RSCS profiles.

Results of the MLD comparison between lidar and radiosoundings are shown in Figure 2; the error bars on the vertical axis represents the standard deviation of the MLDs retrieved from the 15 1-min profiles. For each of the lidar analysis methods, a good agreement was found with correlation coefficients larger than 0.960. The smallest standard deviation is found for the IPM, with a value of 82 m, whereas it is equal to 89 and 101 m, respectively, for the GM and the LGM. Both the GM and LGM retrieve a higher MLD than the IPM, which is normal, since the inflection point of the first derivative is found just before its minimum (for the LGM, this is also true: only the distances change, not the relative position of the points between each other). However, the most remarkable result is that the number of points of the MLD from the radiosoundings within the error bar of the IPM is 1.5 to 2 times larger than for the GM or the LGM. Approximately two thirds of the MLDs from the radiosoundings are within the $h_{IPM}$ error bar. In the next section, the results from the three methods are

discussed, together with their criteria of application and their limitations. Finally, in Section 3.3, the whole database is processed only with the IPM.

### 3.2. Data process and limitations

In order to deliver a lidar ML climatology in Barcelona and to fully test the IPM identifying its advantages and limitations, the analysis was extended to all lidar data available from May 2000 to December 2002 (162 measurement days with 660 profiles averaged over 30 min). We discuss first the results of the three methods on two diurnal cycle measurement days (a simple autumn case and a complex spring case) with complementary information such as synoptic maps, backtrajectories and radiosoundings.

Kinematic backtrajectories were calculated with version 4 of the Hybrid Single-Particle Lagrangian Integrated Trajectory model (HYSPLIT), version 4, developed by the National Oceanic and Atmospheric Administration (NOAA)'s Air Resources Laboratory (ARL) (Draxler and Hess, 1998; Draxler and Rolph, 2003; Rolph, 2003). In the autumn case, meteorological data used for trajectory computation comes from the FNL archives maintained by the ARL (available online at http://www.arl.noaa.gov/ss/transport/archives.html). The FNL data are a product of the Global Data Assimilation System (GDAS), which uses the Global spectral Medium Range Forecast (MRF) model to assimilate multiple sources of measured data and forecast meteorology. Resolution is approximately 190 km in the horizontal with 12 vertical layers on constant pressure surfaces from 1000 to 50 hPa. Because synoptic backtrajectories associated with stagnant situations do not represent the detailed movement of the air masses, and mesoscale effects may not be captured by the analyses from which the trajectories are calculated, in the spring case, the meteorological data used for trajectory computation were derived from a high resolution (9 km, 29 $\sigma$-layers) numerical simulation from the PSU/NCAR Mesoscale Model 5 (MM5), version 3, release 4 modelling system (Dudhia, 1993; Dudhia et al., 2001). Two nested domains were selected and one-way nesting approach was used. Initialization and boundary conditions were introduced with analysis data of the AVN global model. The physics options used for the simulations were the Gayno-Seaman planetary boundary-layer scheme based on Mellor-Yamada turbulent kinetic energy prediction (Gayno et al., 1994), the Kain–Fritsch cumulus scheme (Kain and Fritsch, 1993), the Dudhia simple ice moisture scheme and the cloud-radiation scheme.

Additional information is provided by the temporal evolution of the MLD. Indeed, to be sure to present physically meaningful results, a cross-comparison of the temporal evolution of the MLD was made. This means that, after the first evaluation of the MLD, the plots of Figures 3d and 5d are generated to check the temporal consistency between successive heights.

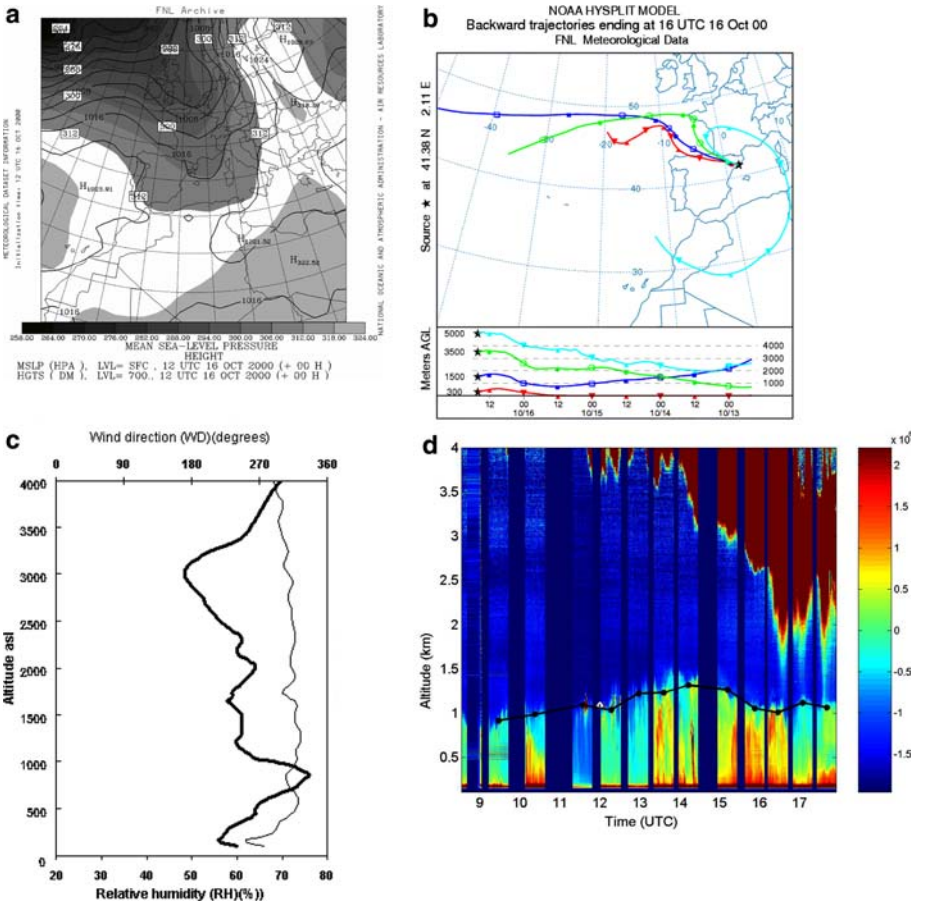


*Figure 3.* 16 October 2000: (a) mean sea level (MSL) pressure and 700 hPa geopotential height at 1200 UTC; (b) 4-day backtrajectories arriving at 300, 1500, 3500 and 5000 m at 1600 UTC over Barcelona; (c) relative humidity (thick solid line) and wind direction (thin solid line) from the radiosounding at 1200 UTC; (d) 1-min resolution diurnal cycle of the RSCS. The black dots indicate the MLD retrieved by the IPM. The white diamond indicates the MLD from the 1200 UTC radiosounding using the Richardson number method.

On 16 October 2000 the Azores anticyclone extended over the Atlantic Ocean south–west from the IP (Figure 3a), and the Barcelona area was influenced by the southern edge of a low pressure system located over the north Atlantic, inducing west to north–west flows (see backtrajectories in Figure 3b and radiosounding in Figure 3c). The 1-min resolution diurnal cycle, which is shown in Figure 3d depicts the ML development from 0830 to 1800 UTC; some thin clouds are observed at the top of the ML just before noon (dark red spot). A thick elevated layer of 2–3 km depth is detected by the lidar at an altitude of 5 km in the morning and 3 km in the afternoon. Backtrajectory analysis clearly identifies the Saharan origin

of the upper airmasses. Saharan dust layers reach the north-eastern IP predominantly when low-pressure systems are located to the west or south-west of the IP, or when the north African anticyclone shifts to the east or south-east of the IP, or by the combination of both cyclonic and anticyclonic systems (Rodriguez et al., 2001; Pérez et al., 2003). This case is an unusual Saharan dust intrusion into the Barcelona free troposphere. Nevertheless, the diurnal cycle (Figure 3d) shows the typical autumn/winter ML development over the area under west to north–west flows. The absolute minimum of the first derivative detects the "real" transition zone between the ML and the FT in all cases, hence the first criterion can be used: the MLD corresponding to $h_{\mathrm{IPM}}$ is given by the minimum of the second derivative just below $h_{\mathrm{GM}}$. To illustrate this case, we plot in Figure 4a the 30-min RSCS profile, together with the profiles from the three derivative methods between 1202 and 1231 UTC. There is absolutely no ambiguity on the retrieval of $h_{\mathrm{GM}}$ and therefore neither on $h_{\mathrm{IPM}}$. Figure 4b shows the 15-min RSCS between 1202 and 1216 UTC. The MLDs retrieved by the three methods are reported in the figure: $h_{\mathrm{GM}} = 1111$ m, $h_{\mathrm{IPM}} = 1093$ m and $h_{\mathrm{LGM}} = 1123$ m, while the radiosounding delivers MLD = 1084 m at 1200 UTC. The temporal variation of the signal within the ML due to the shorter time scale of the convective motions highlights the drawback of the integration time on the MLD retrieval accuracy. Within 30 min the instantaneous MLD can change significantly as the difference between Figure 4a and b shows: integrating over 30 min instead of 15 min lowers the MLD by about 40–50 m on average.

We now turn to a complex situation as an example of the difficulties that often appear when the previous methods are applied to the Barcelona lidar profiles. For 30 May 2002 (Figures 5 and 6), the mean sea-level pressure distribution at 1800 UTC (Figure 5a) features the influence of the southern edge of an anticyclone located over western Europe inducing weak pressure gradient conditions over the region, and the formation of the typical Iberian thermal low with its corresponding relative high pressure area above the western Mediterranean Basin (WMB). The air masses arriving at low levels at 1200 UTC had previously circulated anticyclonically over the WMB, while the upper levels suggested a peninsular origin. The 284-m agl backtrajectory captures the sea-breeze flows over the coast; arrival directions of the backtrajectories are confirmed by the radiosounding in Fig 5c: south to south–west sea-breeze flows up to 600 m and south–west to west flows from 600 to 4000 m. Under such sea-breeze conditions, a TIBL may form as previously observed by Soriano et al. (2001). The wind profile of the radiosounding and the 984-m agl backtrajectory at 1200 UTC show that the dense aerosol layer observed at about 1000 m (see the 1-min resolution diurnal cycle of the RSCS in Figure 5d) in the morning derives

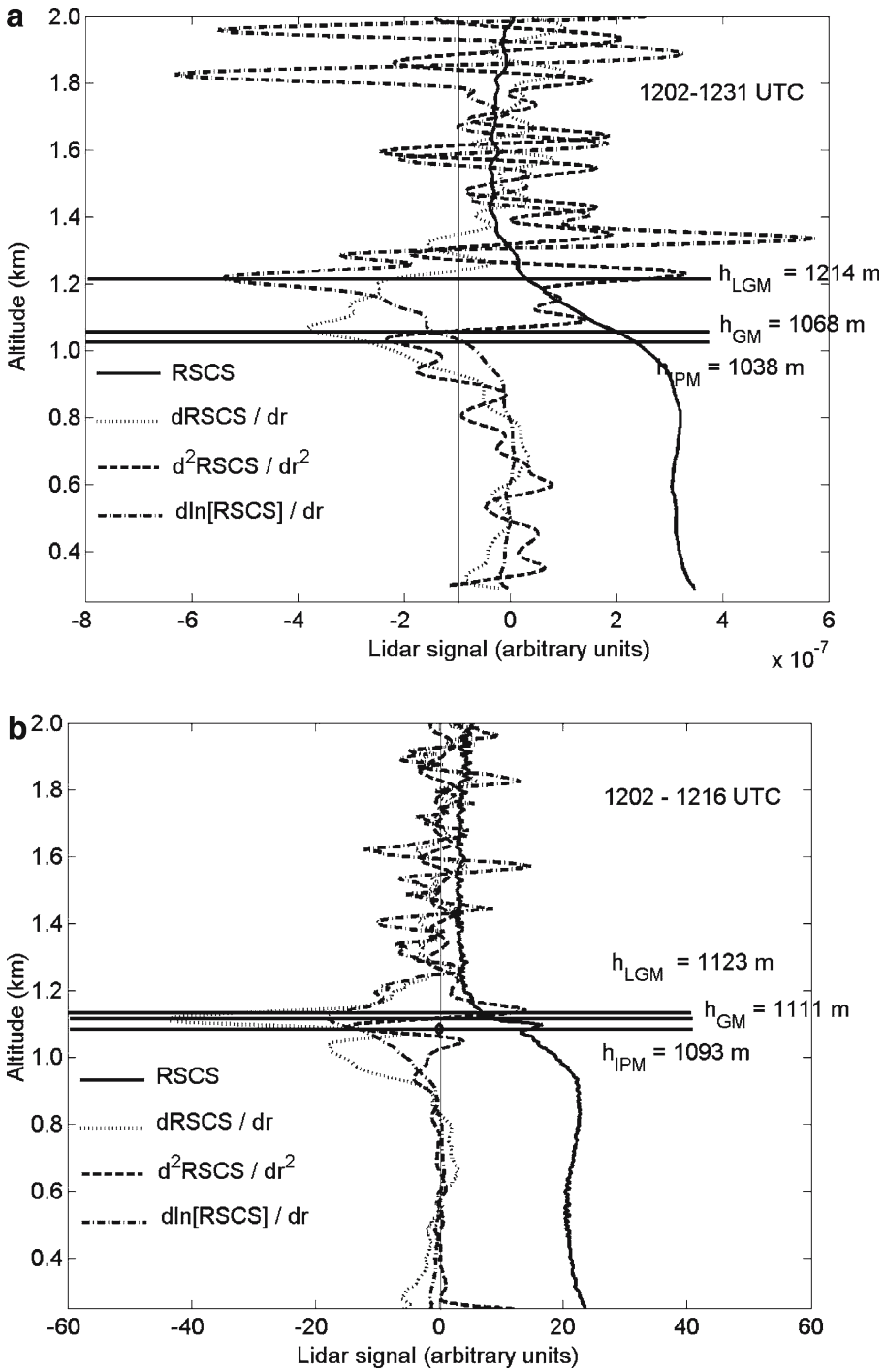


*Figure 4.* (a) 30-min integrated RSCS profiles on 16 October 2000 between 1202 and 1231 UTC, and (b) 15-min integrated RSCS profiles on 16 October 2000 between 1202 and 1216 UTC. The black diamond represents the MLD (1084 m) from the radiosounding at 1200 UTC.

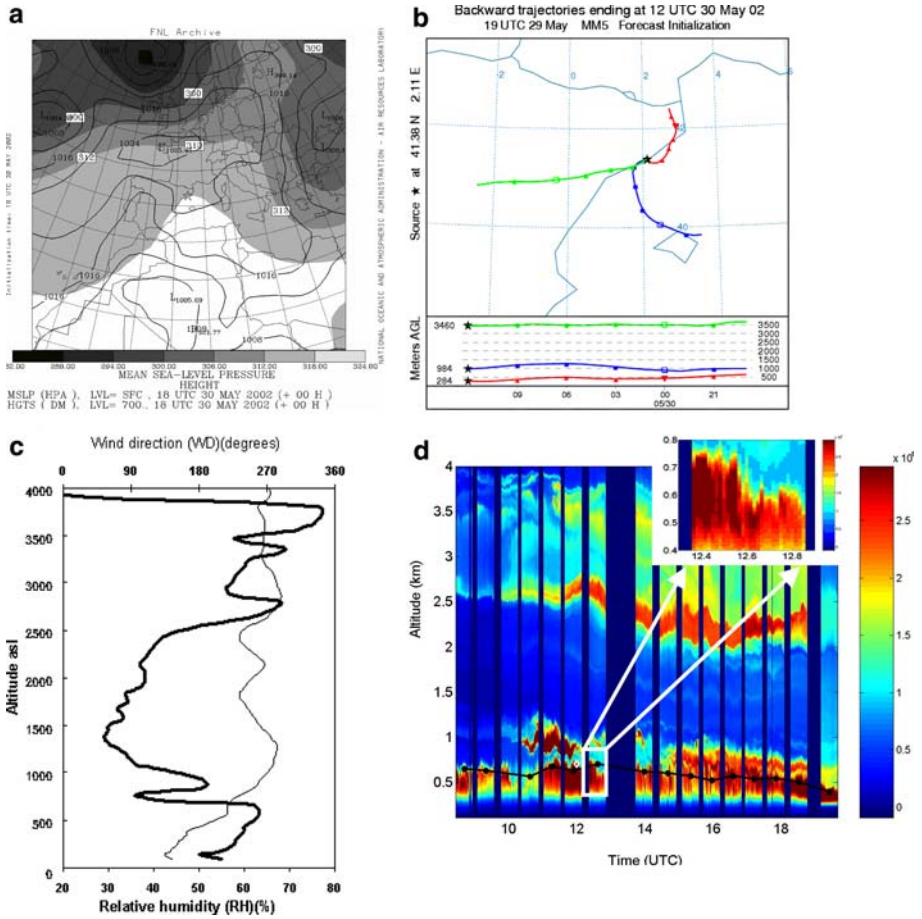


*Figure 5.* 30 May 2000: (a) MSL pressure and 700 hPa geopotential height at 1800 UTC; (b) 18-h backtrajectories arriving at 284, 984 and 3460 m at 1200 UTC over Barcelona; (c) relative humidity (thick solid line) and wind direction (thin solid line) from the radiosounding at 1200 UTC; (d) 1-min resolution diurnal cycle of the RSCS. The black dots indicate the MLD retrieved by the IPM. The white diamond indicates the MLD from the 1200 UTC radiosounding using the Richardson number method.

from the WMB. Relative humidity values (Figure 5c) correlate very well with the layers detected by the lidar. Humidity effects can be important in the lidar data through a swelling of the aerosols and an increase of their effective cross-section. Figures 6a, c and d show the 30-min RSCS profiles, together with the profiles from the three derivative methods at 1139, 1222, and 1543 UTC, respectively. Each profile shows a multi-layer structure below 1500 m. Figure 6a depicts the results at 1139 UTC. The absolute minimum of the first derivative fails and detects the top of the elevated layer at 923 m. The inversion of the upper layer has a sharper signal

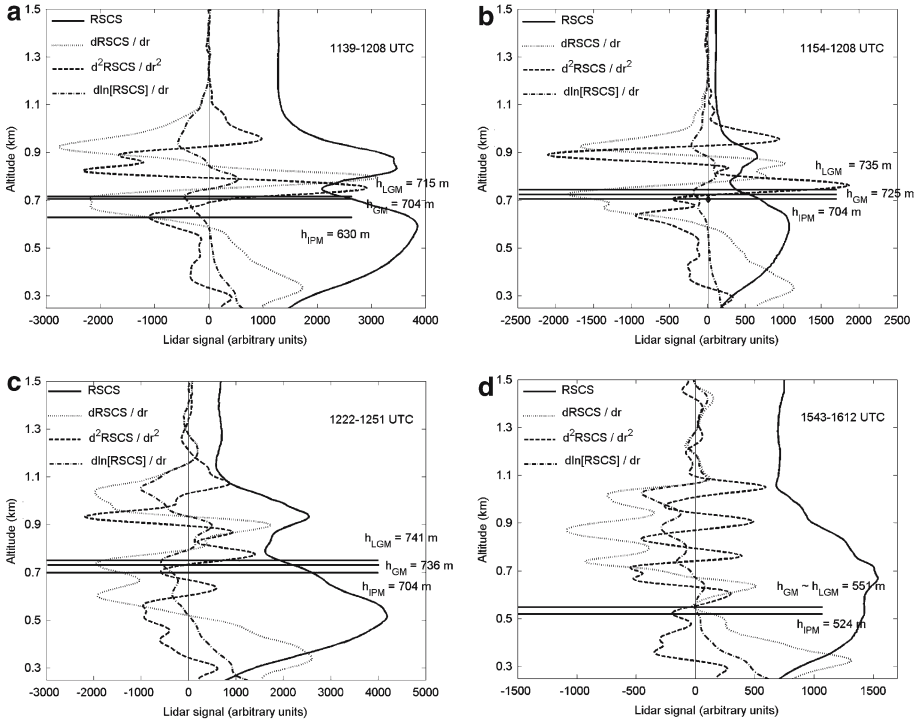


*Figure 6.* 30-min integrated RSCS profiles on 30 May 2002 (a) at 1139, (c) 1222, and (d) 1543 UTC. (b) is the 15-min integrated RSCS profiles on 16 October 2000 between 1154 and 1208 UTC. The black diamond represents the MLD (703 m) from the radiosounding at 1200 UTC.

decrease. In this case, we use the second criterion: the MLD (at 630 m) is given by the minimum of the second derivative below the lowest negative peak of the first derivative. This is confirmed by the radiosounding (Figure 5c). Figure 6b shows the 15-min RSCS between 1154–1208 UTC. The MLDs retrieved by the three methods is reported in the Figure: $h_{GM} = 725$ m, $h_{IPM} = 704$ m and $h_{LGM} = 735$ m while the radiosounding delivers MLD = 703 m at 1200 UTC. As for Figures 4a and b, note that integrating over 30 min instead of 15 min lowers the MLD of about 60 m. At 1222 UTC (Figure 6c), the absolute minimum of the first derivative also fails. The lowest negative peak of the first derivative leads to $h_{GM} = 736$ m and therefore a lower $h_{IPM}$ at 704 m. However the largest negative peak of the second derivative would have led to MLD = 561 m. The sequence from 1222 to 1251 UTC (zoomed in Figure 5d) seems to be split in two: a first group of profiles with a transition at around 725 m, and a second group with a transition around 600 m. The IPM only detects an "averaged" height (704 m) from the 30-min integrated profile, which is closer to 725 m than 600 m. The first group of profiles (1222–1236 UTC)

features a sharper signal decrease around 725 m than the second one (1237–1251 UTC) around 600 m. While the first group can be interpreted as the core of a rising thermal penetrating into the capping inversion, the second group may be the result of downmixing of FT air into the ML. Downdrafts are in general less clearly defined, because they are not directly buoyantly driven. In these downdraft regions, the detected MLD is lower and the transition zone is wider than in the adjacent updrafts. Again, this case shows the drawback of the integration time in the ML retrieval accuracy. At 1543 UTC (Figure 6d), the upper layer is almost completely coupled to the ML and even shows higher RSCS values, but a first small decrease in the RSCS still allows the detection of the MLD (524 m) as being the minimum of the second derivative just below the lowest negative peak of the first derivative. The top of the upper layer is located at 832 m. In the climatological context, if we had considered a single 30-min measurement, one could have stated that the MLD is located at 832 m (the inflection point just below the absolute minimum of the first derivative) arguing that the lowest negative peak of the first derivative could be attributed to inhomogeneities within the ML. This situation points out the importance of following the temporal evolution of the ML through the day. Thus, the diurnal cycle (Figure 5d) allows the connection between the ML and the upper layer to be followed, and the proper minimum located.

Finally, independently of the season, some multi-layer cases related to Saharan dust intrusion or re-circulation of pollutants could not be solved by neither of the methods because the ML was fully connected to the upper layer. In these cases, the GM and LGM detected the top of the first disconnected layer (usually much higher than the "real" transition zone) corresponding to the first decrease of the RSCS; and the IPM detected the lowest negative peak at an altitude lower than $h_{GM}$, corresponding to an inflection point of the first derivative that is decreasing but with a positive sign. Even though in some cases the gradient of the signal weakened around $h_{IPM}$, no conclusion could be drawn from the lidar profiles alone. In these cases, not even the third criterion (if GM fails, $h_{IPM}$ corresponds to the lowest negative peak of the second derivative) could be used. These cases are unsolved cases when analysing lidar profiles from RSCS only. Considering these results and the comments from Section 1, the IPM is then applied to the whole database to retrieve the MLD (see below).

### 3.3. Mixed-Layer depth in Barcelona between 2000 and 2002

Among the 660 measurements made over 162 days, a comparison of the retrieved MLD was made for a certain portion of the diurnal cycle. The period of maximum insolation running from 1000 to 1500 UTC was chosen, which corresponds to the unstable thermal stratification. Figure 7 shows the

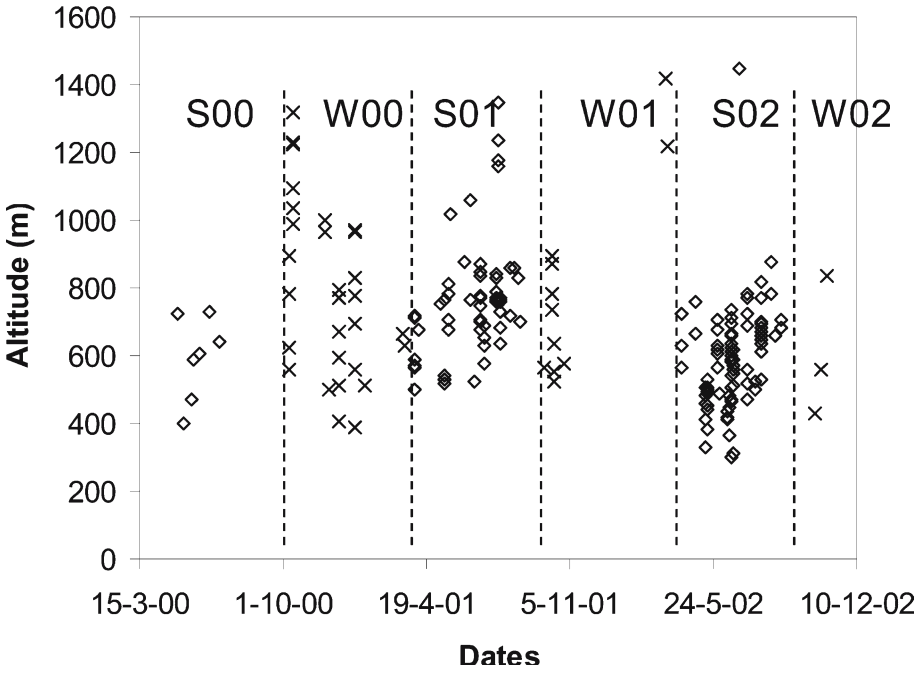


*Figure 7.* Mixed-layer depth as a function of day of the year between May 2000 and December 2002. Diamonds indicate summer measurements (S) and crosses indicate winter measurements (W).

MLD in Barcelona retrieved by the IPM over the period May 2000–December 2002. Two seasons are distinguished: summer (from April to September) and winter (from October to March). The MLD oscillates between 300 and 1450 m in summer and between 390 and 1420 m in winter. The standard deviation for this portion of the day is 180 and 256 m, respectively, in summer and winter. Within the framework of EARLINET (Bösenberg et al., 2003), most stations showed a clear annual cycle with higher values in summer than in winter. For example, in Hamburg it has been shown that, on average, this cycle follows quite well a sine function with maximum values at the beginning of July and lowest values at the beginning of January (Matthias and Bösenberg, 2002). In Figure 7, no significant differences are observed between summer and winter, even though higher values would be expected in summer. This was also the case for Athens (Greece) and Lecce (Italy), which are also coastal stations (Matthias et al., 2004). Furthermore, in Barcelona the average MLD in summer is even smaller than the average MLD in winter. The limited growth of the ML in summer is partly caused by the amplified compensatory subsidence over the Mediterranean sea and its coastal areas, attributable to the combined sea breeze and upslope flows plus the formation of the Iberian thermal low over the central plateau (Millán

et al., 1992; 1997). Generalized subsidence due to the Azores anticyclone and compensatory subsidence from the Iberian thermal low over the WMB represent the synoptic and large mesoscale phenomena that may explain the small growth of the ML. Millán et al. (1992, 1997) have documented the first rapid rise of the MLD during the morning followed by the sinking of its capping inversion during the afternoon. Lidar profiles in Figure 6 follow this pattern. Additionally, sea breezes introduce cool and stable air over the coast. As the column of air advects downwind and warms, the temperature difference between the air and the ground lessens. As a result, the heat flux at the ground decreases, the ML warms less rapidly, and the rise rate of the MLD is reduced (Stull, 1988). Generally, the TIBL does not extend all the way to the top of the marine air associated with the intruding air mass, so the remainder of the cool air mass above the TIBL and below the return flow acts as a barrier for the TIBL vertical development. The TIBL deepens with distance downwind of the shoreline: in our case the retrieved MLD is referred to a point located at about 5 km from the shore.

## 4. Conclusions

The EARLINET climatological database has been thoroughly analyzed in terms of mixed-layer depth (MLD) determination in Barcelona using three derivative methods (gradient method, inflection point method and logarithm gradient method) applicable to single lidar profiles. The methods are based on the determination of the strongest negative gradient of the backscattered lidar signal. As demonstrated in Section 3.1, the inflection point method (IPM) gives the best results when comparing with the Richardson number method, which is widely used to estimate the MLD from radiosoundings. The two other methods give a slightly higher MLD. To estimate $h_{\mathrm{IPM}}$, three criteria were adopted: (1) if the absolute minimum of the first derivative detects correctly the "real" transition zone, $h_{\mathrm{IPM}}$ is the lowest negative peak of the second derivative below the absolute minimum of the first derivative; (2) if the absolute minimum of the first derivative does not detect correctly the "real" transition zone, $h_{\mathrm{IPM}}$ is the lowest negative peak of the second derivative below the lowest negative peak of the first derivative; (3) if the gradient method (GM) fails, $h_{\mathrm{IPM}}$ is the lowest negative peak of the second derivative. It stands out from these criteria that to be able to judge for the correctness of the "real" transition zone detected by the GM, additional information is needed. Therefore, if possible one should (1) use complementary data such as synoptic observations, backtrajectories and radiosoundings, and (2) cross-compare the MLD found with the temporal evolution of the MLD (only lidar data are needed for that). These new contributions help to overcome most of the ambiguities found.

Limitations of the IPM are found in the presence of elevated aerosol layers whenever the inversion capping of the mixed layer is weak. In these cases, small aerosol gradients between the ML and the upper layer are much harder to detect than those from the elevated layers, which exhibit large aerosol and humidity gradients with respect to their surrounding. Layering is a recurrent pattern in Barcelona. Under strong insolation and weak synoptic forcing, sea breezes and mountain-induced winds develop to create re-circulations of pollutants along the coast. Layers are formed when aerosols are injected from the mountains into the return flow at various heights and distances from the coast. Synoptic observations and back-trajectories are essential to understand the meteorological context that can support advective transport or past accumulation processes. Single lidar analysis can introduce large biases in the MLD determination and diurnal cycle measurements are strongly required. The retrieval methods for the MLD cannot be easily automated because the cross-comparison of the temporal evolution of the MLD is a key aspect of its retrieval: it guarantees temporal coherency between successive MLD calculations. The MLD from one radiosounding (or more), taken as a reference, helps in validating the correctness of the temporal evolution of the MLD. Around noon, the ML changes quite rapidly and the analysis of 30-min integrated profiles sometimes shows large differences against 5 and 15-min integrated profiles. This highlights the drawback of the integration time on the MLD retrieval accuracy: the IPM will only detect a "temporal averaged" height. The MLD cross-comparison between lidar and radiosounding measurements among all the inter-compared methods may well be influenced by atmospheric decorrelating effects taking place over the 30-min lidar integration time, particularly between 1000 and 1500 UTC, when the boundary layer has a stronger evolution. Thus, it is necessary that the methodological analysis includes a "discard" procedure to cope with time-punctual specific uncorrelated scenes, such as those arising in cases where an aerosol layer is coupled to the ML above. A methodological hint arising from Section 3.2 is to increase the correlation coefficient of the MLD cross-comparison by the temporal variance computed over the 30-min integrated profiles, since temporal decorrelation of the MLD is a major error source in some of the analyzed profiles.

Among the 660 measurements made over 162 days, the MLD during the period of maximum insolation (from 1000 to 1500 UTC) oscillated, in a statistical sense, between 300 and 1450 m in summer and between 390 and 1420 m in winter. The standard deviation is 180 and 256 m, respectively, in summer and winter. In summer, low values (mainly limited to 400–800 m asl) are associated to compensatory subsidence over the Mediterranean Sea and to TIBL formation: the cool sea-breeze incursion limits the vertical growth of the TIBL, which grows with distance downwind the

coastline. There is a significant differential trend when compared with other continental European cities such as Paris or Hamburg (Bösenberg and Matthias, 2003). The analysis of complex patterns such as those occurring in Barcelona requires a progressive incorporation of new methodologies to the already existing ones along the points suggested in the examples presented in this work.

## Acknowledgements

The authors thank Prof. Comerón, as well as the anonymous reviewers for their valuable comments. They wish to acknowledge the following entities for partially supporting the research work and lidar systems developed at UPC: European Union under the EARLINET contract EU EVR1-CT-1999-40003 and FEDER funds, and MCYT (Spanish Ministry of Science and Technology) under the grant REN2003-09753-CO2-02. ESA and MCYT are also thanked respectively for the external postdoctoral fellowship and the *Ramón y Cajal* position hold by M. Sicard.

## References

Barros, N., Toll, I., Soriano, C., Jiménez, P., Borrego, C., and Baldasano, J. M.: 2003, 'Urban Photochemical Pollution in the Iberian Peninsula: the Lisbon and Barcelona Airsheds', *J. Air and Waste Manag. Assoc*. **53**, 347–359.

Boers, R., Spinhirne, J. D., and Hart, W. D.: 1988, 'Lidar Observations of the Fine-Scale Variability of Marine Stratocumulus Clouds', *J. Appl. Meteorol*. **27**, 797–810.

Bösenberg, J., Ansmann, A., Baldasano, J. M., Balis, D., Böckmann, C., Calpini, B., Chaikovsky, A., Flamant, P., Hagard, A., Mitev, V., Papayannis, A., Pelon, J., Resendes, D., Schneider, J., Spinelli, N., Trickl, T., Vaughan, G., Visconti, G., and Wiegner, M.: 2001, 'EARLINET: A European aerosol research lidar network', in A. Dabas, C. Loth and J. Pelon (eds.), *Advances in Laser Remote Sensing – Selected papers presented at the 20th ILRC*, Vichy (France), July 10–14, 2000, Ecole Polytechnique, Palaiseau, France, pp. 155–158.

Bösenberg, J. and Matthias, V.: 2003, 'EARLINET: A European Aerosol Research Lidar Network to Establish an Aerosol Climatology', in *Final Report for the Period February 2000 to February 2003*, Max-Planck-Institut für Meteorologie, Hamburg, Germany, 212 pp.

Brooks, I. M.: 2003, 'Finding Boundary Layer Top: Application of a Wavelet Covariance Transform to Lidar Backscatter Profiles', *J. Atmos. Oceanic Technol*. **20**, 1092–1105.

Cohn, S. A. and Angevine, W. M.: 2000, 'Boundary-Layer Height and Entrainement Zone Thickness Measured by Lidars and Wind Profiling Radars', *J. Appl. Meteorol*. **29**, 1233–1247.

Deardorff, J. W., Willis, G. E., and Stockton, B. H.: 1980, 'Laboratory Studies of the Entrainment Zone of a Convectively Mixed Layer', *J. Fluid. Mech*. **100**, 41–64.

Draxler, R. R. and Hess, G. D.: 1998, 'An Overview of the Hysplit_4 Modelling System for Trajectories, Dispersion, and Deposition', *Austr. Meteorol. Mag*. **47**, 295–308.

Draxler, R. R., and Rolph, G. D.: 2003, *HYSPLIT (HYbrid Single-Particle Lagrangian Integrated Trajectory) Model access via NOAA ARL READY Website (http://www.arl.noaa.gov/ready/hysplit4.html)*, NOAA Air Resources Laboratory, Silver Spring, MD.

Dudhia, J.: 1993, 'A Non-Hydrostatic Version of the Penn State-NCAR Mesoscale Model: Validation Tests and Simulation of An Atlantic Cyclone and Cold Front', *Mon. Wea. Rev.* **121**, 1493–1513.

Dudhia, J., Gill, D., Guo, Y., Manning, K., and Wang W.: 2001, *PSU/NCAR Mesoscale Modeling System Tutorial Class Notes and User's Guide: MM5 Modeling System Version 3*, Mesoscale and Microscale Meteorology Division, National Center for Atmospheric Research, Boulder, CO (June 18, 2001), http://www.mmm.ucar.edu/mm5/.

Dupont, E.: 1991, *Etude méthédologique et expérimentale de la couche limite atmosphérique par télédétection laser*, Ph.D. dissertation., Université Pierre et Marie Curie, Paris, France, 220 pp.

Flamant, C., Pelon, J., Flamant, P. H., and Durand, P.: 1997, 'Lidar determination of the entrainement zone thickness at the top of the unstable marin atmospheric boundary-layer', *Boundary-Layer Meteorol.* **83**, 247–284.

Gayno, G. A., Seaman, N. L., Lario, A. M., and Stauffer, D. R.: 1994, 'Forecasting Visibility Using a 1.5-order Closure Boundary Layer Scheme in a 12-km Nonhydrostatic Model', in: *AMS Tenth Conference on Numerical Weather Prediction*, American Meteorological Society, 45 Beacon St., Boston, MA, pp. 18–20.

Hägeli, P., Steyn, D. G., and Strawbridge, K. B.: 2000, 'Spatial and Temporal Variability of Mixed-layer Depth and Entrainment Zone Thickness', *Boundary-Layer Meteorol.* **97**, 47–71.

Hayden, K. L., Anlauf, K. G., Hoff, R. M., Strapp, J. W., Bottenheim, J. W., Wiebe, H. A., Froude, F. A., Martin, J. B., Steyn, D. G., and McKendry, I. G.: 1997, 'The Vertical Chemical and Meteorological Structure of the Boundary Layer in the Lower Fraser Valley during Pacific '93', *J. Atmos. Environ.* **31**, 2089–2105.

Holzworth, C. G.: 1967, 'Mixing Depths, Wind Speeds and Air Pollution Potential for Selected Locations in the United States', *J. Appl. Meteorol.* **6**, 1039–1044.

Hooper, W. P., and Eloranta, E. W.: 1986, 'Lidar Measurements of Wind in the Planetary Boundary Layer: The Method, Accuracy and Results from Joint Measurements with Radiosonde and Kytoon', *J. Climate Appl. Meteorol.* **25**, 990–1001.

Jorba, O., Pérez, C., Rocadenbosch, F., and Baldasano, J. M.: 2004, 'Cluster Analysis of 4-day Backtrajectories Arriving in the Barcelona Area (Spain) From 1997 to 2002', *J. Appl. Meteorol.* **43**, 887–901.

Kain, J. S., and Fritsch, J. M.: 1993, 'Convective Parameterisation for Mesoscale Models: The Kain-Fritsch Scheme,' in K. A. Emanuel and D. J. Raymond (eds.), *The Representation of Cumulus Convection in Numerical Models*, American Meteorological Society, 45 Beacon St., Boston, pp. 246.

Martín-Vide, J.: 1987, *Característiques climatològiques de la precipitació en la franja costera mediterrània de la Península Ibèrica*, PhD. Dissertation, Institut Cartogràfic de Catalunya, Barcelona, Spain, 245 pp.

Matthias, V. and Bösenberg, J.: 2002, 'Aerosol climatology for the planetary boundary layer derived from regular lidar measurements', *Atmos. Res.* **63**, 221–245.

Matthias, V., Balis, D., Bösenberg, J., Eixmann, R., Iarlori, M., Komguem, L., Mattis, I., Papayannis, A., Pappalardo, G., Perrone, M. R., and Wang, X.: 2004, 'Vertical aerosol distribution over Europe: Statistical analysis of Raman lidar data from 10 European Aerosol Research Lidar Network (EARLINET) stations', *J. Geophys. Res.* **109**, D18201, doi:10.1029/2004JD004638.

Melfi, S. H., Spinhirne, J. D., Chou, S. H., and Palm, S. P.: 1985, 'Lidar Observation of the Vertically Organized Convection in the Planetary Boundary Layer Over the Ocean', *J. Clim. Appl. Meteorol.* **24**, 806–821.

Menut, L., Flamant, C., Pelon, J., and Flamant, P. H.: 1999, 'Urban Boundary-Layer Height Determination from Lidar Measurements Over the Paris area', *Appl. Opt.* **38**, 945–954.

Millán, M. M., Artinñano, B., Alonso, L., Castro, M., Fernandez-Patier, R., and Goberna, J.: 1992, 'Mesometeorological Cycles of Air Pollution in the Iberian Peninsula', *Air Pollution Research Report 44*, Commission of the European Communities, Brussels, Belgium, 219 pp.

Millán, M., Salvador, R., and Mantilla, E.: 1997, 'Photooxidant Dynamics in the Mediterranean Basin in Summer: Results From European Research Projects', *J. Geophys. Res.* **102**, 8811–8823.

Pérez, C., Jiménez, P., Rocadenbosch, F., and Baldasano, J. M., 2003, 'Lidar Observations of Saharan Dust and Regional Pollution Events Over the Northeastern Iberian Peninsula in the Frame of EARLINET', in *American Association for Aerosol Research 2003 – Abstract of the 22nd Annual Conference*, Anaheim, California, October 20–24, 2003, pp. 89.

Pérez, C., Sicard, M., Jorba, O., Comerón, A., and Baldasano, J. M.: 2004, 'Summertime Re-Circulations of Air Pollutants Over the North-Eastern Iberian Coast Observed From Systematic EARLINET Lidar Measurements in Barcelona', *Atmos. Environ.* **38**, 3983–4000.

Rocadenbosch, F., Sicard, M., Comerón, A., Baldasano, J. M., Rodríguez, A., Agishev, R., Muñoz, C., López, M. A. and García-Vizcaino, D.: 2002, 'The UPC Scanning Raman Lidar: An Engineering Overview', in L. Bissonnette, G. Roy, and G. Vallée (eds.), *Lidar Remote Sensing in Atmospheric and Earth Sciences – Reviewed and revised papers presented at the 21st ILRC*, Québec (Canada), July 8–12, 2002, Defence R & D Canada – Valcartier, Val-Bélair, Canada, pp. 69–70.

Rodríguez, S., Querol, X., Alastuey, A., Kallos, G. and Kakaliagou, O.: 2001, 'Saharan Dust Contribution to PM10 and TSP Levels in Southern and Eastern Spain', *Atmos. Environ.* **35**, 2433–2447.

Rolph, G. D.: 2003, *Real-time Environmental Applications and Display sYstem (READY) Website (http://www.arl.noaa.gov/ready/hysplit4.html)*, NOAA Air Resources Laboratory, Silver Spring, MD.

Seibert, P., Beyrich, F., Gryning, S. E., Joffre, S., Rasmussen, A., and Tercier, P.: 1998, 'Mixing layer depth determination for dispersion modelling', *COST Action 710 – Final Report. Harmonisation of the pre-processing of meteorological data for atmospheric dispersion models, Report of Working Group 2*, Office for Official Publications of the European Communities, Luxembourg, 431 pp.

Seibert, P., Beyrich, F., Gryning, S. E., Joffre, S., Ramussen, A., and Tercier, P.: 2000, 'Review and Intercomparison of Operational Methods for the Determination of hte Mixing Height', *Atmos. Environ.* **34**, 1001–1027.

Senff, C., Bösenberg, J., Peters, G., and Schaberl, T.: 1996, 'Remote Sesing of Turbulent Ozone Fluxes and the Ozone Budget in the Convective Boundary Layer with DIAL and Radar-RASS: A Case Study', *Contrib. Atmos. Phys.* **69**, 161–176.

Sicard, M., Pérez, C., Comerón, A., Baldasano, J. M., and Rocadenbosch, F.: 2003, 'Determination of the Mixing Layer Height from Regular Lidar Measurements in the Barcelona Area', in K. P. Schäfer, A. Comerón, M. R. Carleeer, and R. H. Picard, (eds.), *Proc. SPIE* 5235-66, ISSN 0277-786X, ISBN 0-8194-5118-5, Barcelona, Spain, September 8–12, 2003, SPIE, PO Box 10, Bellingham, WA, pp. 505–516.

Soriano, C., Baldasano, J. M., Buttler, W. T., and Moore, K.: 2001, 'Circulatory Patterns of Air Pollutants Within the Barcelona Air Basin in a Summertime Situation: Lidar and Numerical Approaches', *Boundary-Layer Meteorol.* **98**, 33–55.

Steyn, D. G., Baldi, M., and Hoff. R.: 1999, 'The Detection of Mixed Layer Depth From Lidar Backscatter Profiles', *J. Atmos. Oceanic Tech*. **16**, 953–959.

Stull, R. B.: 1988, *An Introduction to Boundary Layer Meteorology*, Kluwer Academic Publishers, Dordrecht, The Netherlands, 670 pp.

Vogelezang, D. H. P., and Holtslag, A. A. M.: 1996, 'Evaluation and Model Impacts of Alternative Boundary-Layer Height Formulations', *Boundary-Layer Meteorol*. **81**, 245–269.